Robotics and Autonomous Systems 60 (2012) 1472–1483

Contents lists available at SciVerse ScienceDirect

Robotics and Autonomous Systems

journal homepage: www.elsevier.com/locate/robot

A biomimetic underwater microrobot with multifunctional locomotion

Shuxiang Guo [a,b], Liwei Shi [a,*], Nan Xiao [a], Kinji Asaka [c]

[a] Faculty of Engineering, Kagawa University, 2217-20, Hayashi-cho, Takamatsu, 761-0396, Japan

[b] College of Automation, Harbin Engineering University, 145 Nantong Street, Harbin, Heilongjiang, 150001, China

[c] Health Research Institute, National Institute of Advanced Industrial Science and Technology (AIST), 1-8-31 Midorigaoka, Ikeda, Osaka 563-8577, Japan

ARTICLE INFO

Article history:
Received 5 December 2011
Received in revised form
26 April 2012
Accepted 28 July 2012
Available online 4 August 2012

Keywords:
Ionic polymer metal composite (IPMC) actuators
Biomimetic underwater microrobot
Micromechanism

ABSTRACT

Underwater microrobots are in urgent demand for applications such as pollution detection and video mapping in limited space. Compact structure, multi-functionality, and flexibility are normally considered incompatible characteristics for underwater microrobots. Nevertheless, to accomplish our objectives, we designed a novel inchworm-inspired biomimetic locomotion prototype with ionic polymer metal composite (IPMC) actuators, and conducted experiments to evaluate its crawling speed on a flat underwater surface. Based on this type of biomimetic locomotion, we introduced a new type of underwater microrobot, using ten IPMC actuators as legs or fingers to implement walking, rotating, floating, and grasping motions. We analysed the walking mechanism of the microrobot and calculated its theoretical walking speed. We then constructed a prototype of the microrobot, and carried out a series of experiments to evaluate its walking and floating speeds. Diving/surfacing experiments were also performed by electrolysing the water around the surfaces of the actuators. The microrobot used six of its actuators to grasp small objects while walking or floating. To implement closed-loop control, we employed three proximity sensors on the microrobot to detect an object or avoid an obstacle while walking.

1. Introduction

The development of microrobots has proceeded rapidly. They are widely used in underwater monitoring operations, including pollution detection, video mapping, and exploration of unstructured underwater environments. However, the electromagnetic structure of traditional motors is difficult to miniaturize. Thus, motors are rarely found in this type of application [1,2], and special actuator materials are used instead. A variety of smart materials, such as ionic polymer metal composite (IPMC), piezoelectric elements, pneumatic actuators, and shape memory alloy (SMA), have been investigated for use as artificial muscles in new types of microrobot [3–5].

Kim et al. proposed an earthworm-like microrobot using SMA actuators [6]. An SMA-based hexapod biomimetic robot was reported [7]. Hadi et al. developed another SMA-actuated robotic module [8]. Shahinpoor et al. employed IPMC as actuators to fabricate a four-finger gripper [9]. With IPMC used as an actuator, Yeom et al. designed a biomimetic jellyfish, which can be activated to mimic real locomotive behaviour with pulse and recovery processes [10]. Zhang et al. developed a new type of fish-like microrobot with swimming, walking, and floating motions, which was actuated by ionic conducting polymer film (ICPF) actuators [11]. Also, Hao et al. designed a miniature fish-like robot, which can be controlled by an infrared remote controller [12].

Although many biomimetic microrobots actuated by smart actuators have been developed in recent years, it is still difficult to develop a microrobot with compact structure, flexibility, and multi-functions, because these characteristics conflict with each other. For this reason, most microrobots lose a compact structure, as they use biomimetic multi-joint legs to improve their flexibility and obtain multi-functions, while some other microrobots give up the flexibility and multi-functions in pursuit of miniaturization.

In this research, IPMC is used as actuator material to develop a microrobot with a compact structure, multi-functionality, and flexibility. The actuation characteristics of IPMC, including a suitable response time, high bending deformation, and long life, show significant potential for the propulsion of underwater microrobots [13–17]. IPMC actuators can be used as artificial muscles to propel robots backwards and forwards, they are mainly used as oscillating or undulating fins for swimming microrobots

* Corresponding author. Tel.: +81 87 864 2356; fax: +81 87 864 2369.
E-mail addresses: guo@eng.kagawa-u.ac.jp (S. Guo), slw8304@hotmail.com, shi@eng.kagawa-u.ac.jp (L. Shi), xiao@eng.kagawa-u.ac.jp (N. Xiao), asaka-kinji@aist.go.jp (K. Asaka).

0921-8890/$ – see front matter © 2012 Elsevier B.V. All rights reserved.
doi:10.1016/j.robot.2012.07.013

when fast response is required [4,5,11,12,18–21]. However, the swimming motion cannot ensure the position precision for the robot. The fish-like robots cannot implement a backward swimming motion, which is essential in limited space. Also, the fish-like propulsion mechanisms just mimic the undulating and oscillatory body/fin motions. It is hard to implement some simple underwater tasks without hands or fingers. So, besides the swimming, some other biomimetic locomotions are required for the microrobot with compact structure, multi-functions, and flexibility.

Nature is the best model for a robot [22]. Creatures give us an abundance of structures for the biomimetic robot design. We have developed several microrobots that employ biomimetic locomotion to implement walking, rotating, floating, and swimming motions. Inspired by the stick insect, an eight-legged microrobot with eight IPMC actuators distributed symmetrically around the microrobot's symmetry centre was developed, which could implement walking, rotating, and floating motions [23]. To improve the floating motion of the stick insect-inspired eight-legged microrobots, a jellyfish-type underwater microrobot with four IPMC legs was developed, which could implement walking and floating/diving motions [24]. The floating motion could be controlled freely by changing the input voltage and frequency. But its flexibility and floating efficiency were not so good. To improve the floating motion and implement fast swimming motion, a jellyfish- and butterfly-inspired underwater microrobot was developed and evaluated [25]. Its body was redesigned as a triangular prism to achieve maximum volume change and a higher floating speed was obtained. However, each of these units implemented only some of these motions. They were unable to carry out simple tasks such as grasping and carrying objects to a desired position, detecting an object, or avoiding an obstacle. With the aim of creating a compact structure with efficient and precise locomotion and multi-functionality, we developed a new inchworm-inspired microrobot with ten IPMC actuators used as legs or fingers. This unit employed four of its actuators to walk, rotate, and float. The other six actuators were utilised to implement grasping. Also, the microrobot could detect the direction and distance of an object, and avoid an obstacle while walking, using three short-range proximity sensors.

In the fundamental research of bio-inspired robots, the developed prototype microrobot shows the feasibility and availability of the proposed biomimetic locomotions, which can guide us in microrobot design. The developed underwater microrobot is driven by a low voltage, which is safe and economical, so it can be used for the amusement application, such as toys or used in the aquarium. With the compact structure, efficient and precise locomotion and multi-functionality, it can also be used for underwater exploration in limited underwater environments in the future. In addition, it shows significant potential for monitoring ocean currents and chemical agents, and studying animal migration, depth measurements and military functions.

The remainder of this paper is divided into five parts. First, we describe the design of an inchworm-inspired biomimetic crawling structure with one DOF, including its walking mechanism, prototype development, and crawling experiments on an underwater plastic surface. Second, we present the design of an improved crawling structure with two DOFs, including the results of crawling and rotating experiments. Third, we introduce a new type of microrobot with compact structure and multi-functional locomotion, analyse the walking mechanism, and calculate its theoretical walking speed. Also, we describe object detection and obstacle avoidance while walking, using three proximity sensors installed in the front part of the microrobot. Fourth, we discuss the development of a prototype of this underwater microrobot, together with a series of experiments to evaluate its walking and floating speeds on a flat underwater surface. Diving/surfacing, grasping and obstacle avoidance experiments are also included. Finally, we present our conclusions.

2. Proposed underwater microrobot with one DOF

2.1. Biomimetic locomotion

Inchworms have smooth, hairless bodies, usually about 25 mm long. Also known as measuring worms, spanworms, or loopers, they lack appendages in their midsections, causing them to have a characteristic looping gait. They have three pairs of true legs at the front end, like other caterpillars, but only two or three pairs of prolegs (larval abdominal appendages) at the rear end [26]. As Fig. 1 indicates, an inchworm moves by drawing its hind end forward while holding on with the front legs, then advancing its front section while holding on with the prolegs.

2.2. Proposed 1-DOF underwater peristaltic structure

Normally, compact structure is a key point in microrobot design. An inchworm-inspired biomimetic locomotion prototype with an IPMC actuator was introduced to implement fast creeping. The design was based on a 1-DOF leg. The structure of the proposed robot is shown in Fig. 2. This robot could only implement crawling motion. The locomotion was accomplished with two components: an actuator and a PET film. The IPMC actuator was 11 mm long, 2 mm wide, and 0.2 mm thick. The ionic polymer metal composite consisted of Au plated on a Nafion^{TM} film.

2.3. Mechanism of peristaltic motion

Fig. 3 shows a one-step cycle of forward crawling. In one step, the microrobot could move a distance d. The crawling speed could be determined by the displacement of the actuator and the frequency of the control signal. We denoted the displacement of the actuator without a payload by d_0, and assumed that the microrobot could move forward with a displacement of d in one step.

2.4. Crawling experiment

The prototype of the 1-DOF crawling structure is shown in Fig. 4. The crawling experiment was carried out on an underwater plastic surface. We applied different voltages and frequencies, and recorded the times required to cover a distance of 50 mm. The experiment was repeated 10 times for every set of control signals to determine the average speed on an underwater plastic surface. The tip displacement of the IPMC decreased as the input frequency increased. Therefore, the microrobot had a maximum walking speed. The experimental results of Fig. 5 indicate that the walking speed was nearly proportional to the input voltage; a maximum speed of 1.41 mm/s was obtained with a control signal of 12 V and 17 Hz.

3. Proposed underwater microrobot with two DOFs

3.1. Proposed 2-DOF underwater crawling structure

The 1-DOF crawling structure was used to implement the characteristic of compactness. Accordingly, we next focused our attention on multi-functionality and flexible locomotion. To implement rotational motion, we improved the 1-DOF crawling structure by using two legs. The resulting structure is shown in Fig. 6. It was 11 mm long, 15 mm wide, and 11 mm high. This microrobot was designed to implement both crawling and rotating motions.

Fig. 1. Photograph of a living inchworm [27].

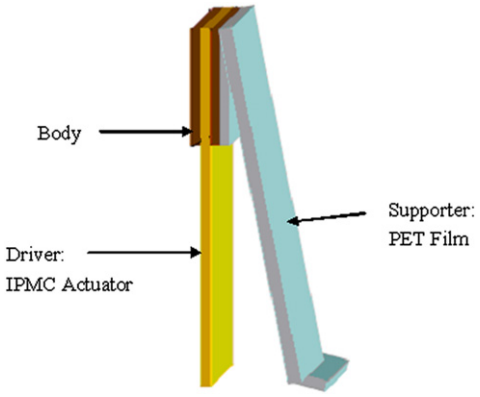

Fig. 2. Proposed 1-DOF crawling structure.

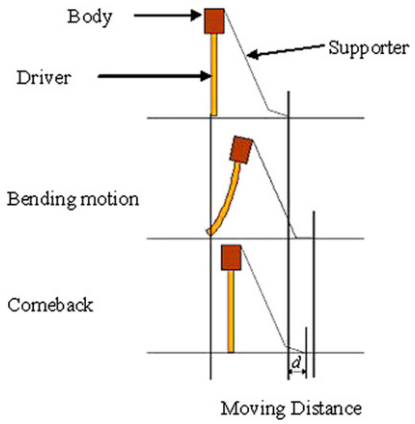

Fig. 3. One-step cycle of crawling motion.

3.2. Rotating experiment

Using its crawling locomotion, the microrobot could implement a rotating motion in either the clockwise or counter-clockwise direction by moving one side forward while holding the other side still. The speed of the rotating motion could be determined by the rotational angle covered in a single cycle and the frequency of the step. The rotating experiment was carried out on the same underwater plastic surface. Here, we simply measured the crawling speed of the moving leg. The experimental results are shown in Fig. 7.

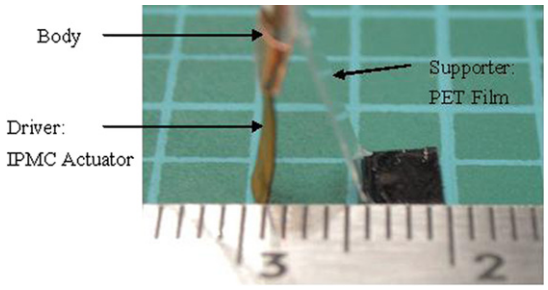

Fig. 4. Prototype of the 1-DOF crawling structure.

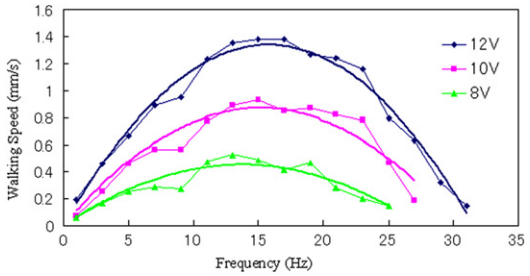

Fig. 5. Experimental speeds measured during crawling motion (1-DOF).

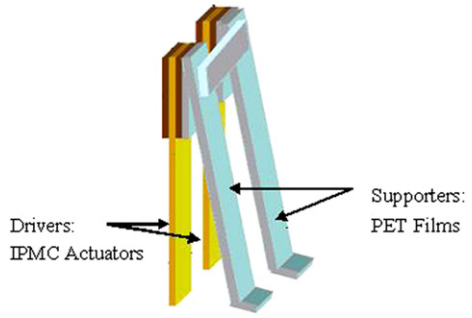

Fig. 6. Proposed 2-DOF crawling structure.

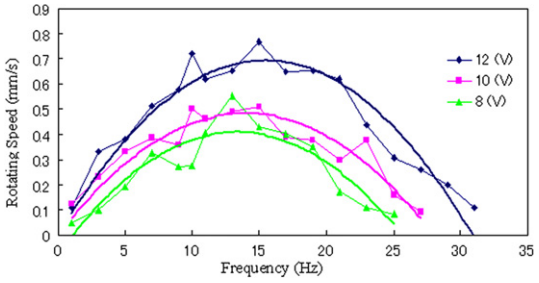

Fig. 7. Experimental speeds measured during rotating motion (2-DOF).

4. Proposed multi-functional underwater microrobot

4.1. Proposed underwater microrobot structure

Based on the validity of inchworm-inspired biomimetic locomotion, we introduced a new type of underwater microrobot, using IPMC actuators as legs or fingers that could implement walking, rotating, floating, and grasping motions. The structure of the proposed biomimetic microrobot is shown in Fig. 8. It was 33 mm long, 14 mm wide, and 14 mm high. The ten IPMC actuators were designated A through J; the sequence of ten legs is shown in Fig. 9. Legs A, B, C, and D were used to realise both walking motion in the longitudinal direction and floating motion. The other six actuators were used either as legs to realise walking motion in the transverse

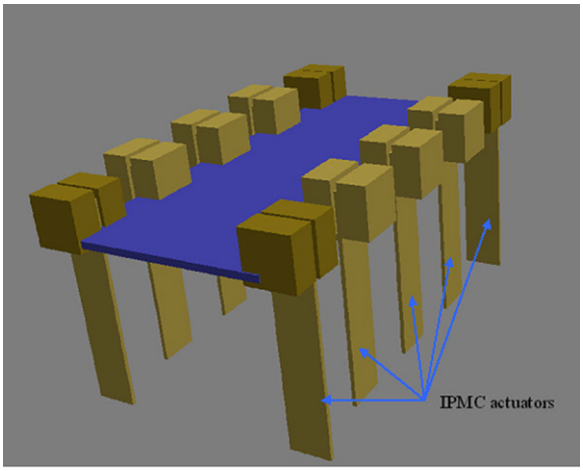

Fig. 8. Proposed biomimetic microrobot.

direction, or as fingers to realise grasping motion. Each of the actuators was 12 mm long, 3 mm wide, and 0.2 mm thick.

4.2. Mechanism of the walking motion

Fig. 10 shows the walking mechanism with one DOF. The two legs had the same oscillating frequency. One leg was called the leading leg, and the other was called the following leg. When the robot walked forward, the phase of the leading leg was 90° behind that of the following leg. Every step cycle of the walking motion could be divided into four periods. The microrobot could move a distance of $2d$ during a single step cycle.

Based on this walking mechanism, our microrobot could realise a walking motion in both the longitudinal and transverse directions, as shown in Fig. 9. When A and C were used as following legs and B and D were used as leading legs, the robot walked in the longitudinal direction. During this motion, the phase of legs B and D lagged that of legs A and C by 90°. When H, I, and J were used as leading legs and E, F, and G were used as following legs, the robot walked in the transverse direction. In this case, the phase of legs H, I, and J lagged that of legs E, F, and G by 90°.

The speed of the walking motion could be determined by the displacement of the drivers and the input frequency. We denoted the displacement of the actuator without payload by d_0, while the displacement of the actuator in an actual application was denoted by d. Because of the payload, water resistance, and other factors, the displacement of the drivers decreased by a non-negligible amount Δd. Thus, the relationship between d_0 and d could be expressed as Eq. (1), and the walking speed could be expressed as Eq. (2), where v is the average speed and f is the frequency of the input signal:

$$d = d_0 - \Delta d \tag{1}$$

$$v = 2\,(d_0 - \Delta d)\,f. \tag{2}$$

4.3. Equivalent cantilever beam modelling

The IPMC beam actuator could be modelled as a supported cantilever beam, as shown in Fig. 11. When the microrobot was crawling, the forces applied to one leg are shown in Fig. 12, where q is the surface tension of the IPMC actuator and F is the resultant force of friction and water resistance on one leg [28,29].

According to cantilever beam theory, the relationship between the deformation curvature $1/\rho(x)$ and the mechanical moment M is given by Eq. (3):

$$\frac{1}{\rho(x)} = \frac{M(x)}{EI} \tag{3}$$

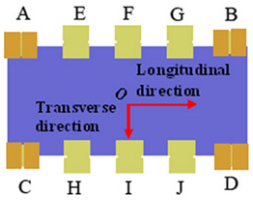

Fig. 9. Sequence of ten legs.

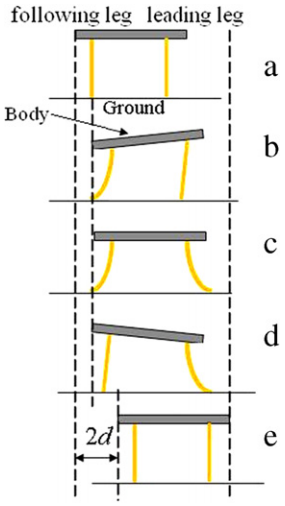

Fig. 10. Microrobot crawling mechanism.

where E is the elastic modulus for IPMC under hydrated conditions and I is the moment of inertia of the equivalent cantilever beam. The mechanical moment M due to IPMC bending is a function of the applied forces [24].

Using the curvature equation of the deflection curve, we obtain Eq. (4):

$$\frac{\frac{d^2w}{dx^2}}{\left[1+\left(\frac{dw}{dx}\right)^2\right]^{3/2}} = -\frac{M(x)}{EI}. \tag{4}$$

For a small deflection of the IPMC actuator, Eq. (4) can be simplified and approximated as Eq. (5):

$$\frac{d^2w}{dx^2} = -\frac{M(x)}{EI}. \tag{5}$$

The tip displacement generated by the surface tension q on one side of the IPMC is denoted by w_q. Hence, the tip displacement without payload $d_0 = w_q$ can be calculated from Eq. (6):

$$d_0 = w_q = \frac{qx^2}{24}(-4lx + 6l^2 + x^2) = \frac{ql^4}{8EI}. \tag{6}$$

The tip displacement generated by the resultant force F on one side is denoted by w_F. Thus, the decrease in the displacement $\Delta d = w_F$ can be calculated using Eq. (7). As a result, the actual deflection d can be obtained from Eq. (8):

$$\Delta d = w_F = \left(-\frac{Fx^3}{6EI} + \frac{Flx^2}{2EI}\right) = \frac{Fl^3}{3EI} \tag{7}$$

$$d = d_0 - \Delta d = w_q - w_F = d_0 - \frac{Fl^3}{3EI}. \tag{8}$$

In order to calculate W_F, the IPMC bending stiffness EI can be obtained from experimental results and the following relationship:

$$I = \frac{b \cdot h^3}{12}. \tag{9}$$

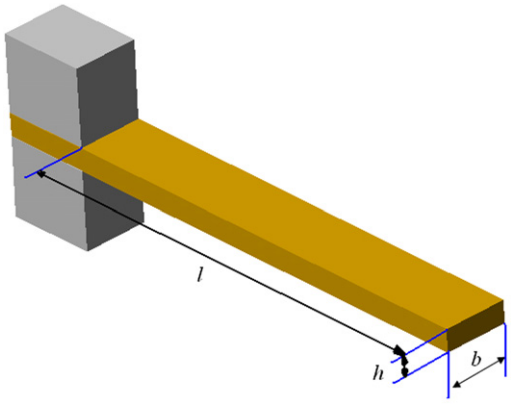

Fig. 11. Equivalent cantilever beam for an IPMC actuator [24].

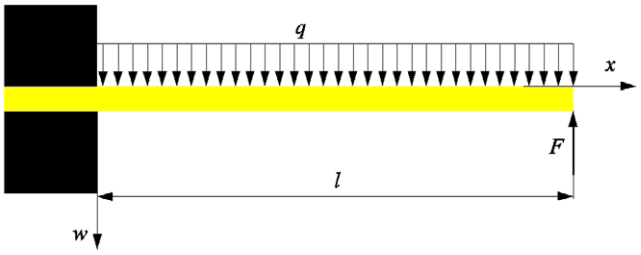

Fig. 12. Forces and deflection of an IPMC actuator in the w direction [24].

The measured value of the elastic modulus E for IPMC under hydrated conditions is about 83 MPa [28]. For cross-sectional dimensions of 0.2 mm × 3 mm, the moment of inertia of IPMC is about 2.0 $mm^4 \times 10^{-3}$ mm^4. The bending stiffness is then 166.0 $mN \cdot mm^2$. For one leg, the force F is frictional, and is given by Eq. (10).

$$F = \mu_s N \tag{10}$$

where N is the positive pressure between the leg and the bottom of the water tank, and μ_s is the coefficient of static friction. Based on the material properties of IPMC and the hard steel bottom, we set $\mu_s = 0.30$ in our experiments. Since the microrobot had a weight of 1.419 g in air and a volume of 0.76 cm^3, its weight in water was 0.659 g, and for one leg, $N = 0.659\ g/4 = 0.165$ g. Hence, the force F on one leg was 0.484 mN. Since the leg length $l = 12$ mm, the force $F = 0.484$ mN, and the bending stiffness of the leg $EI = 166.0\ mN \cdot mm^2$, the decrease in the displacement Δd of the IPMC drivers was 1.68 mm.

We measured the displacement of a single IPMC actuator by applying different signals to simulate the theoretical crawling speed of the microrobot in a water tank. The actuator was 12 mm long, 3 mm wide, and 0.2 mm thick. Fig. 13 shows the experimental tip displacements d_0 of the actuator, recorded at different frequencies and a voltage of 6 V. These results show that the tip displacement decreased as the frequency increased. Therefore, the microrobot had a maximum walking speed. The theoretical walking speed could be calculated using Eq. (2). The simulated results are shown in Fig. 14.

4.4. Mechanism of the rotating motion

Based on the walking mechanism, when A and D were used as following legs and B and C were used as leading legs, one side of the microrobot moved forward and the other side moved backward. As a result, the robot could rotate clockwise. When B and C were used as following legs and A and D were used as leading legs, the microrobot could realise counter-clockwise rotating motion. The speed of the rotating motion could be determined by the rotational angle covered in a single cycle and the frequency of the step.

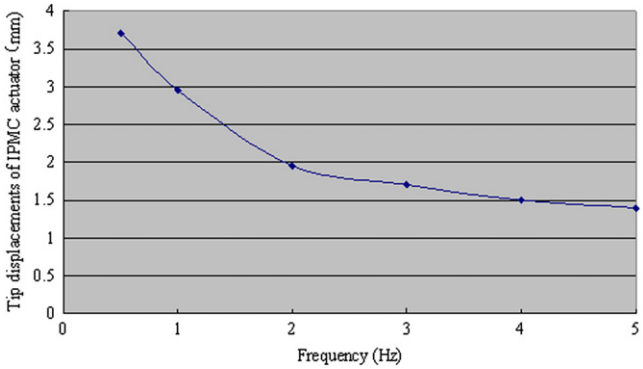

Fig. 13. Tip displacement (d_0) of the IPMC actuator (6 V).

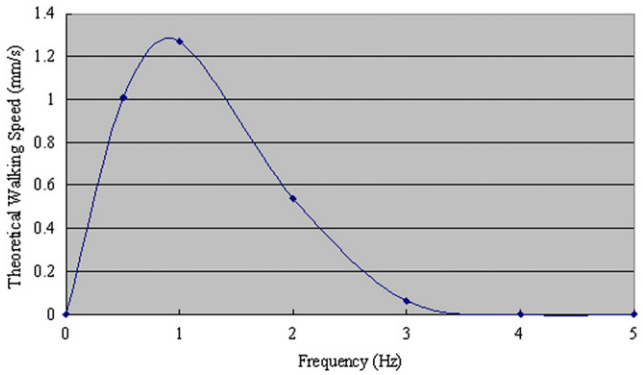

Fig. 14. Theoretical walking speed of the microrobot (6 V).

Table 1
Control strategies for crawling locomotion.

Motions	Following legs	Leading legs
Crawling in the longitudinal direction	A, C	B, D
Crawling in the transverse direction	E, F, G	H, I, J
Clockwise rotation	A, D	B, C
Counter-clockwise rotation	B, C	A, D

A, B, C, D, E, F, G, H, I, and J indicate the legs (see Fig. 9).

Note that we did not use legs E, F, G, H, I, and J to realise rotating motion, since these six actuators were mainly used as fingers for grasping small objects. E, F, and G were designated as one group, and H, I, and J as another group. The actuators in a group were driven by a single control signal. The control strategies for the crawling and rotating motions are listed in Table 1.

4.5. Mechanism of the floating motion

We electrolysed the water around the surfaces of the IPMC actuators by decreasing the frequency of the applied voltage to 0.3 Hz. The buoyancy of the microrobot could be controlled by the resulting change in volume, making it float upward, remain statically buoyant, or sink downward. We used legs A, B, C, and D to electrolyse the water and realise the floating motion. Table 2 lists the control strategies for the floating motion.

4.6. Mechanism of the grasping motion

Legs E through J could be used as fingers to grasp small objects and carry them to a desired location. First, the microrobot positioned itself over the object using legs A through D. Next, leg pairs E–H, F–I, and G–J bent toward each other. The object was then grasped by these six fingers. Finally, while carrying the object, the robot could walk to a desired location or float upward from the bottom of the water tank using legs A, B, C, and D.

Table 2
Control strategies for floating locomotion.

Conditions	Floating motions
$\rho g(V + \Delta V) < mg$	Sinking downward
$\rho g(V + \Delta V) = mg$	Suspended
$\rho g(V + \Delta V) > mg$	Floating upward

ρ is the density of water, g is the acceleration due to gravity, V is the volume of the microrobot, ΔV is the volume of the bubbles, and mg is the weight of the microrobot.

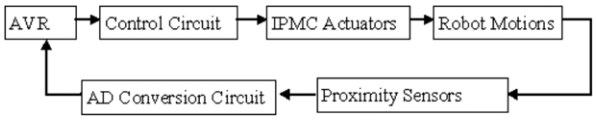

Fig. 15. Control system for the microrobot.

4.7. Control system

4.7.1. Control circuit

In previous research, underwater microrobots simply realised walking, rotating, swimming, or floating motions. However, most of them were driven with an open-loop control [29–32]. For improved motion stability and precision, our robot used three proximity sensors to detect and avoid an obstacle while walking, as shown in Fig. 15. Fig. 16 shows the prototype control system for the microrobot. We used the AVR atmega16 as the control centre, and an electric relay as a circuit changer to vary the input voltages of the ten IPMC actuators. The control signals of the IPMC actuators were all square waves, which could drive the IPMC actuators more efficiently. To accommodate the small size of the microrobot, the proximity sensors must be small and light; as Fig. 17 shows, the proximity sensors used in the present research were 8 mm long and 5 mm wide, with a weight of 0.5 g. The distance measurement range for one sensor was from 0 to 60 mm, and the output voltage ranged from 150 mV to the power voltage.

To determine the available distance between the sensor and an obstacle, we calibrated the proximity sensors in air and in water. The calibration results for one proximity sensor are shown in Fig. 18. As the figure indicates, when the distance between the sensor and the obstacle changed from 60 to 25 mm, the output voltage increased slowly from 0 to 0.2 V. When the distance was less than 25 mm, the output voltage began to increase rapidly. Hence, we set 25 mm as the effective range of a proximity sensor. When the output voltage of a sensor was higher than 0.2 V, we assumed that the sensor had detected an obstacle.

The angle measurement range for one proximity sensor was from -30° to 30°. Thus, we used three proximity sensors to scan the entire front side of the microrobot. The arrangement of the three proximity sensors is shown in Fig. 19. According to the values received from the three sensors, the microrobot was able to judge the direction and distance of an obstacle, and altered its motion accordingly [3,33].

4.7.2. Flow chart of the obstacle avoidance program

A flow chart of the obstacle avoidance program is shown in Fig. 20. In the main function, we initialised the states of Port A, Port B, and the UART. In the circle program, the AVR sent the order codes to the AD conversion circuit. The output voltages of the three proximity sensors were converted to digital values between 0 and 255. According to the order codes, the AD conversion circuit returned these digital values to the AVR [19,34,35]. At a distance of 25 mm, the output voltage for one sensor was 0.2 V, and the digital value at this judgment point was calculated as 20. When one of the values from the AD conversion circuit was larger than 20, we assumed that this sensor had detected an obstacle. The

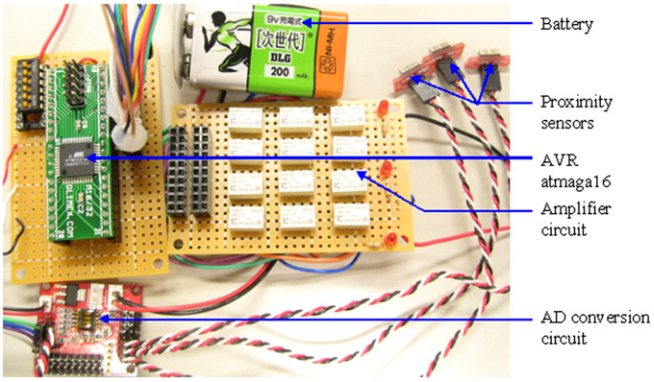

Fig. 16. Prototype control system.

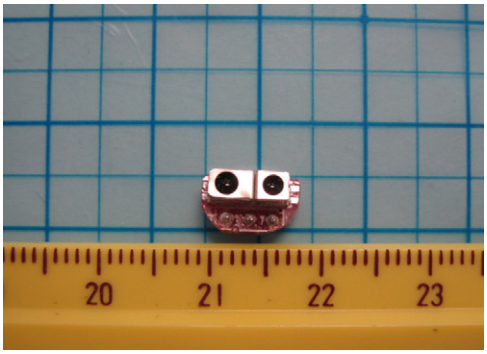

Fig. 17. Proximity sensor.

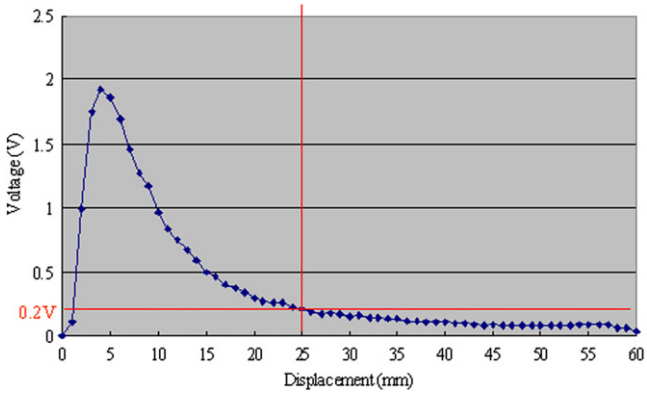

Fig. 18. Calibration results for one proximity sensor.

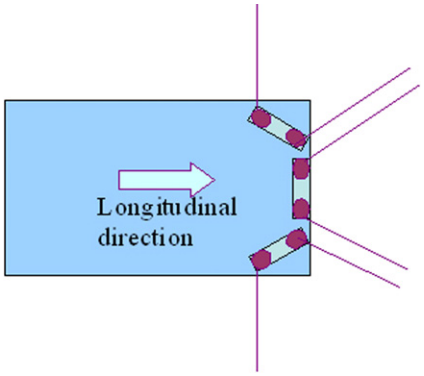

Fig. 19. Arrangement of the three proximity sensors.

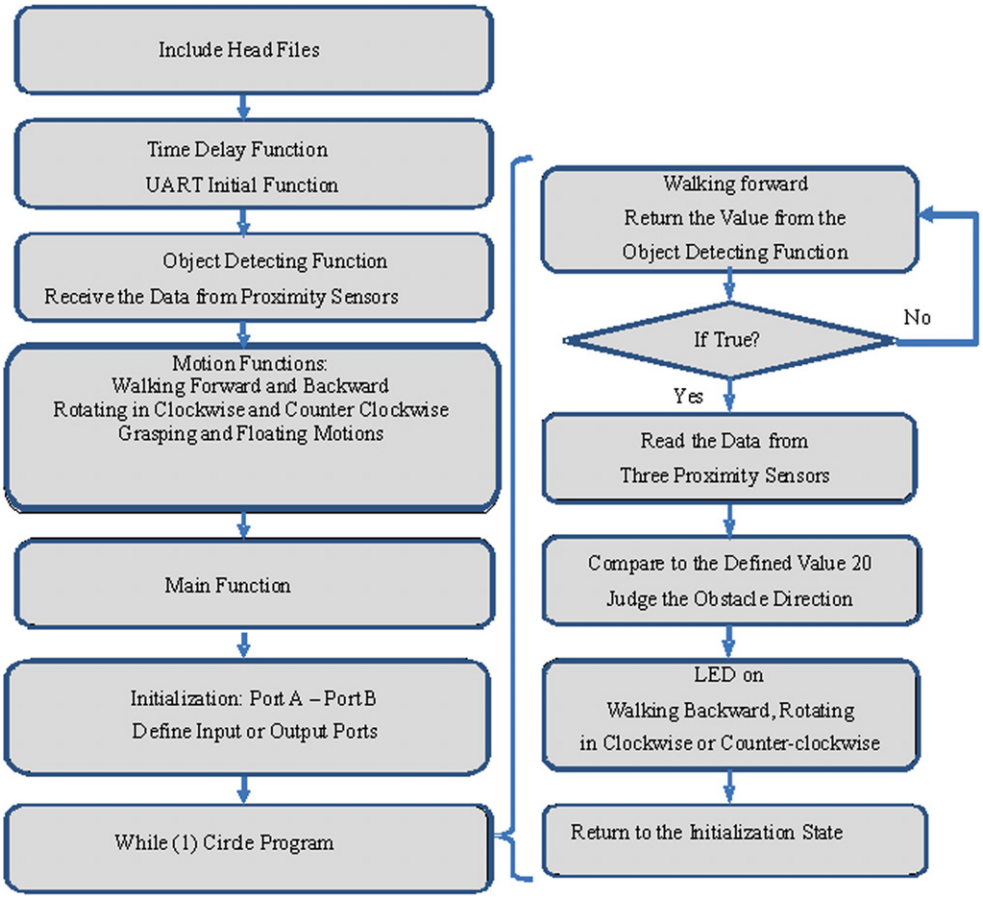

Fig. 20. Flow chart of the obstacle avoidance program.

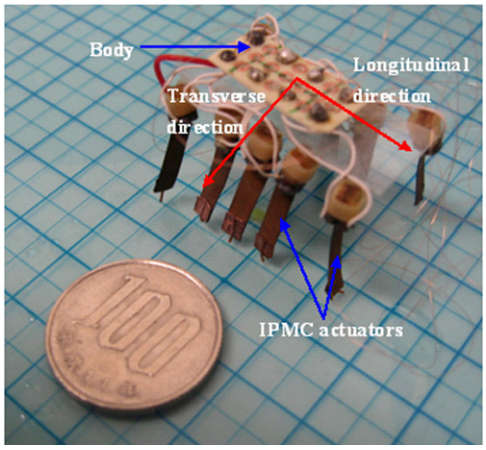

Fig. 21. Prototype of the ten-legged microrobot.

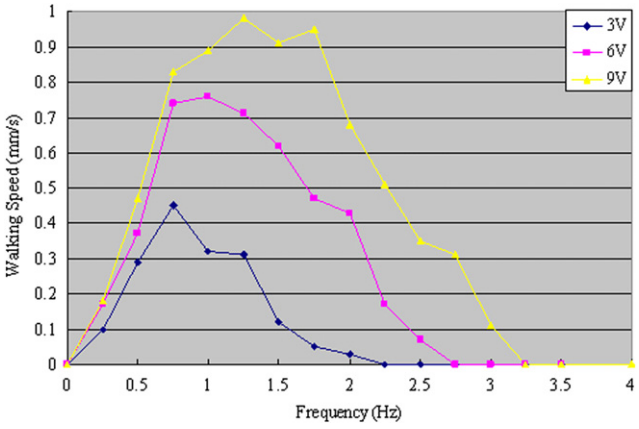

Fig. 22. Experimental walking speed results in air.

direction and distance of an obstacle could be determined based on the output of the three sensors. The microrobot could then change its motion, either by walking backward, or rotating clockwise or counter-clockwise.

5. Microrobot prototype and experiments

5.1. Prototype of the ten-legged microrobot

The prototype microrobot is shown in Fig. 21. It had ten actuators attached to a film body with wooden clips. The control signals were transmitted by enamel-covered wires. The guide wires were 600 mm long, and the copper conductor was 0.03 mm in diameter. The wires were soft enough for the resistance to be ignored. The IPMC legs had spikes to prevent them from sliding.

5.2. Walking experiment in air

Legs E, F, G, H, I, and J were used to implement walking motion in the transverse direction, while legs A, B, C, and D were used to implement walking motion in the longitudinal direction. Since both walking motions had the same driving principle, we chose the longitudinal direction as a sample to estimate the walking speed of the robot. To evaluate walking locomotion in the longitudinal direction, we first conducted an experiment in air. We recorded the times required to walk a distance of 50 mm, using different applied

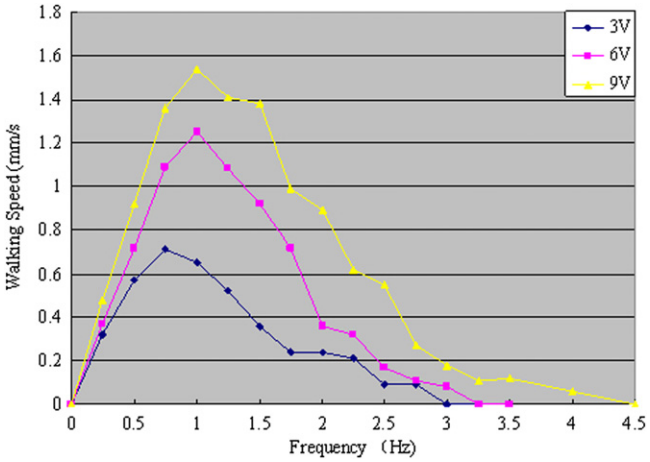

Fig. 23. Experimental walking speed results on the flat underwater surface.

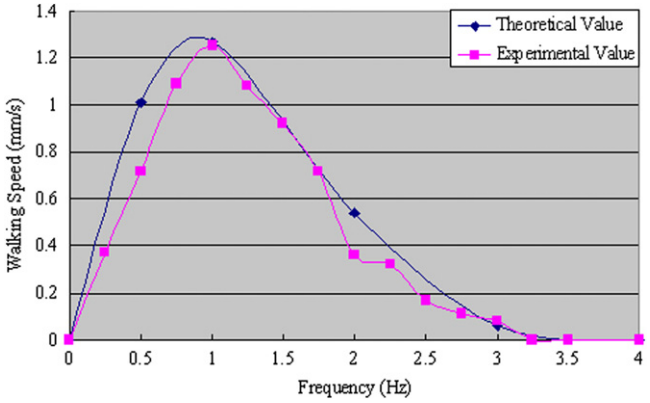

Fig. 24. Relationship between the theoretical and experimental values (6 V).

signal voltages and frequencies. The experiment was repeated 10 times for every set of control signals to determine the average speed in air. The experimental results for the longitudinal direction are shown in Fig. 22. We can see that: (1) in air, the walking speed increased with the input voltage; (2) at 9 V, a maximum speed of 0.98 mm/s was attained at 1.25 Hz; (3) at 6 V, a maximum speed of

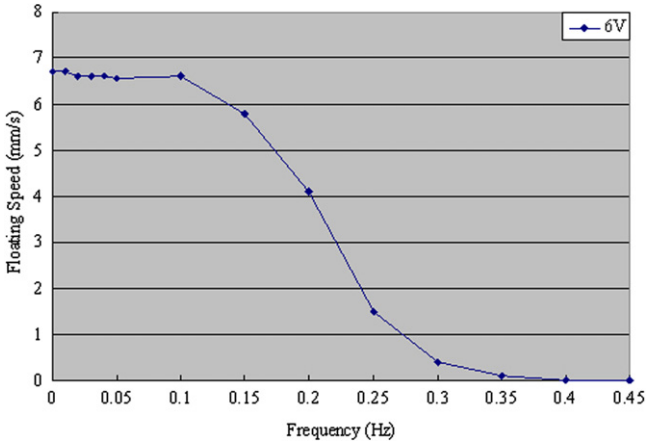

Fig. 26. Experimental floating speed results without payloads (6 V).

0.76 mm/s was attained at 1 Hz; and (4) at 3 V, a maximum speed of 0.46 mm/s was attained at 0.75 Hz. When the frequency was higher than 3.25 Hz, the walking speed approached 0.

5.3. Walking experiment on a flat underwater surface

A walking experiment was also carried out on a flat underwater surface. For comparison with the results of the previous experiment, here we also chose the longitudinal direction as the sample to estimate the walking speed of the robot. Using different applied signal voltages and frequencies, we recorded the times required to walk a distance of 50 mm. This experiment was also repeated 10 times for every set of control signals to determine the average speed. We then calculated the average walking speeds on the flat underwater surface. The experimental results for the longitudinal direction are shown in Fig. 23. We can see that: (1) in water, the walking speed increased with the voltage; (2) at 9 V, a maximum speed of 1.54 mm/s was attained at 1 Hz; (3) at 6 V, a maximum speed of 1.25 mm/s was attained at 1 Hz; and (4) at 3 V, a maximum speed of 0.71 mm/s was attained at 0.75 Hz. When the frequency was higher than 4.5 Hz, the walking speed approached 0. Owing to the buoyancy of water, the decrease in the displacement Δd of the drivers was less than the decrease recorded in air. As a result, the walking speeds were higher in water than in air. The speed

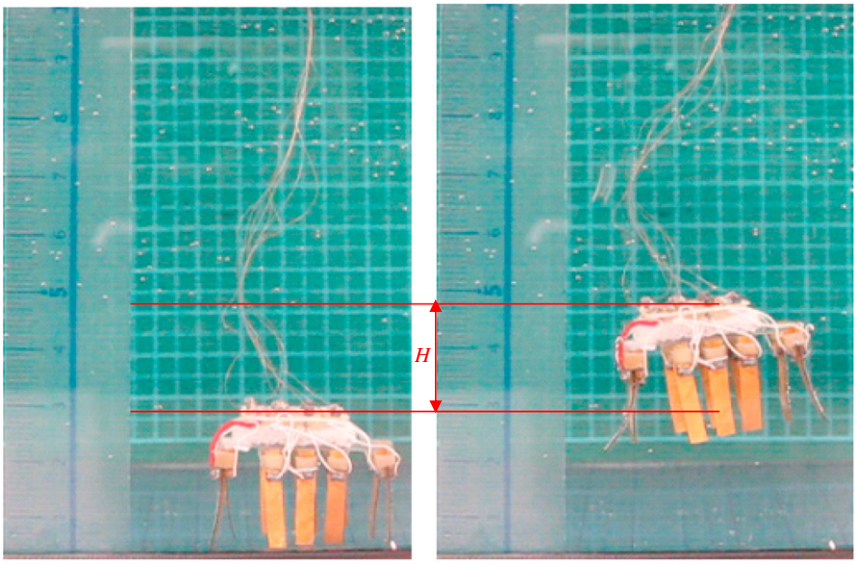

(a) Initial position. (b) Floating motion.

Fig. 25. Floating experiment.

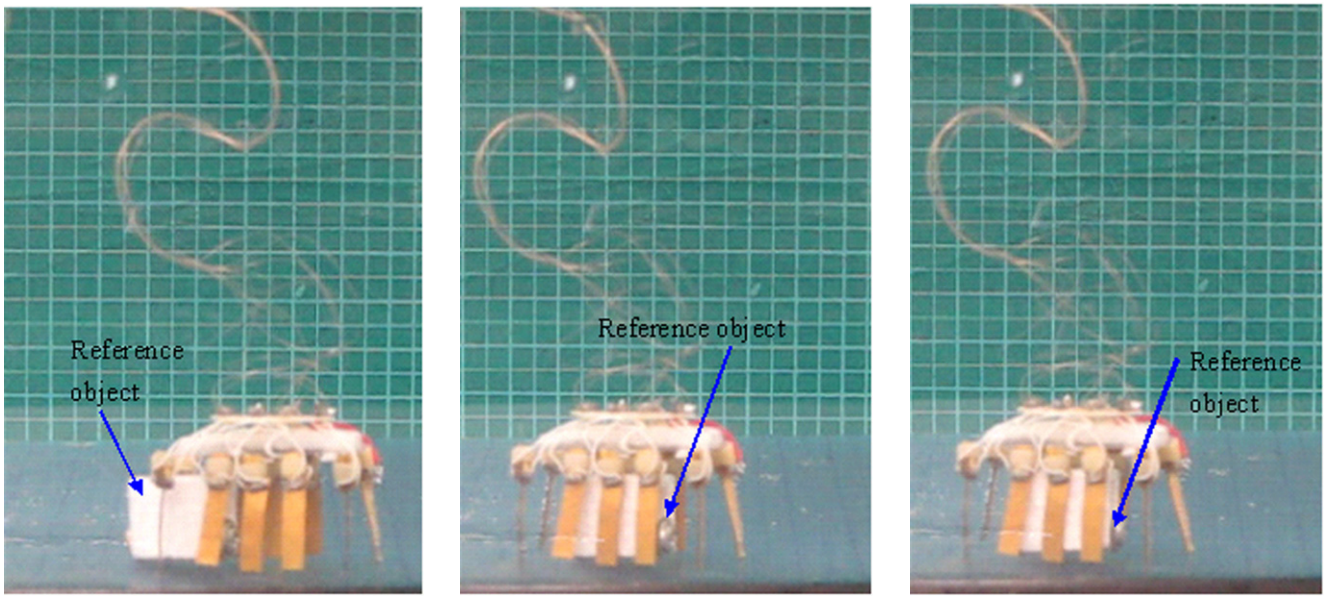

(a) Initial position. (b) Walking motion. (c) Grasping motion.

(d) Floating motion.

Fig. 27. Grasping and floating experiment.

curves obtained in air and on the flat underwater surface were coincident in trend.

The displacement of the IPMC actuators would be smaller in actual applications due to loading, slippage, and the short response time at high frequencies. Therefore, although the experimental results fit the theoretical results very well, some differences still exist, as indicated in Fig. 24.

5.4. Floating experiment without payloads

Legs A, B, C, and D were used to realise floating locomotion. In the experiment, we varied the frequency from 0 to 0.45 Hz for an applied voltage of 6 V. The water around the IPMC surfaces was then electrolysed. If the voltage was cut off while the microrobot was floating upward, the upward motion gradually ceased and the robot started to sink. Fig. 25 shows the floating motion. The experimental floating speeds without payloads are shown in

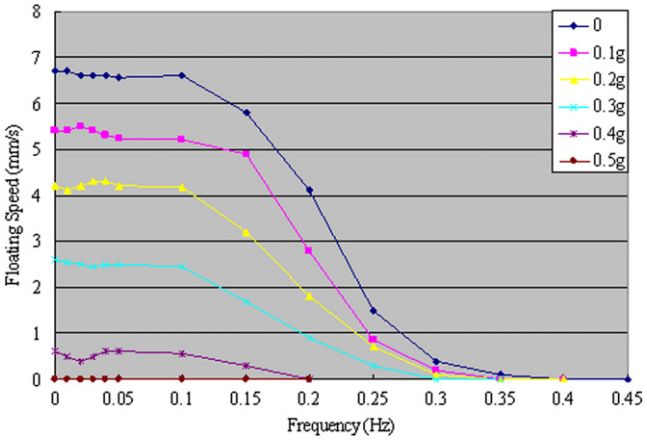

Fig. 28. Experimental floating speed results with payloads (6 V).

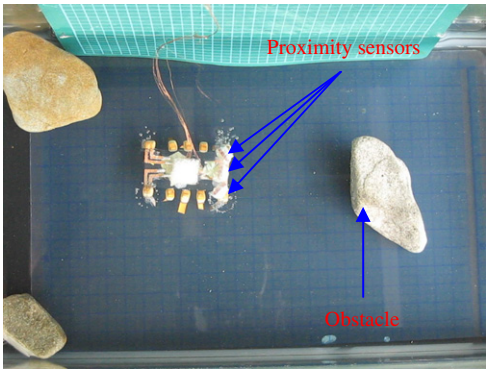

(a) Initial state.

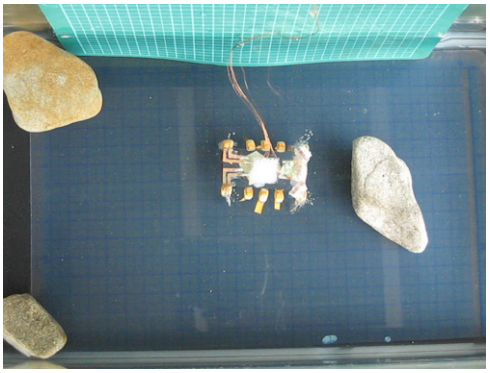

(b) Walking motion.

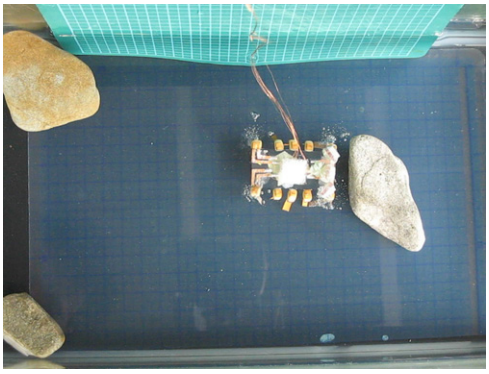

(c) Detected the obstacle.

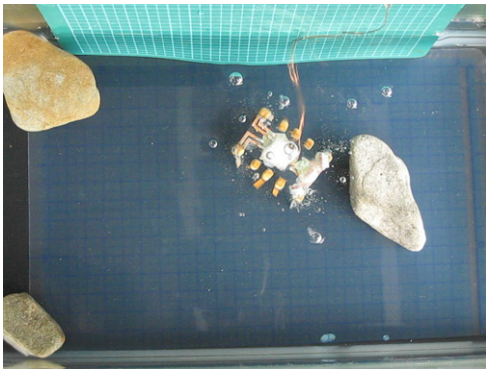

(d) Rotating motion.

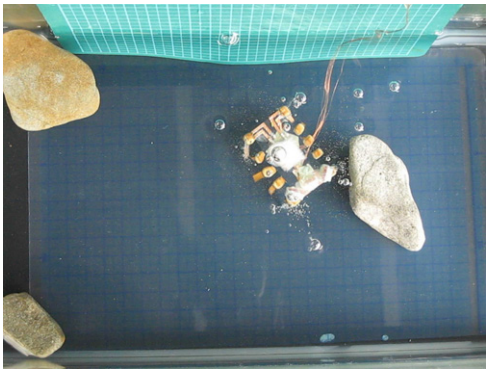

(e) Left sensor detected the obstacle.

(f) Not detected.

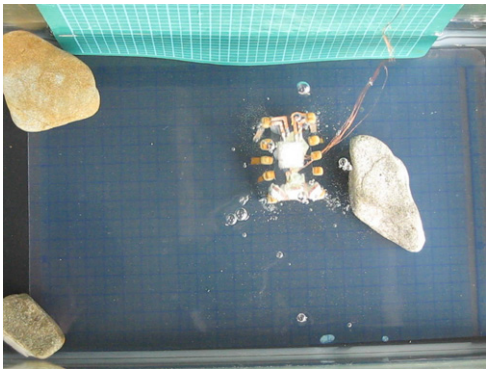

(g) Walking motion.

(h) Final position.

Fig. 29. Obstacle avoidance experiment.

Fig. 26 for an input voltage of 6 V. From 0 to 0.1 Hz, the floating speed varied slightly in the vicinity of 6.6 mm/s. The maximum floating speed approached 6.8 mm/s at 0 Hz. When the frequency was higher than 0.1 Hz, the floating speed began to decrease. When the frequency was higher than 0.4 Hz, the microrobot was no longer able to float upward. At a frequency of 0 Hz, the IPMC actuator could be permanently deformed. Hence, we did not use a DC signal to electrolyse the water and realise floating motion.

5.5. Grasping and floating experiments with payloads

Legs E, F, G, H, I, and J could be used as fingers to grasp small objects. Fig. 27 shows the walking, grasping, and floating motions of the microrobot. First, the microrobot walked toward the object using legs A, B, C, and D. Second, leg pairs E–H, F–I, and G–J were bent toward each other, and the object was grasped by the six fingers. Third, the control signals of legs A, B, C, and D were changed to 0.05 Hz to electrolyse the water around the IPMC surfaces, and the microrobot began to float while grasping the object. In order to evaluate its floating ability, we placed payloads on the robot while it was floating. The experimental conditions were the same as those of the experiments without payloads. The experimental floating speeds with payloads are shown in Fig. 28. The maximum speed while grasping a 0.1 g object approached 5.5 mm/s. The maximum payload with which the robot was able to float upward was 0.3 g. All curves decreased when the frequency was higher than 0.1 Hz.

5.6. Obstacle avoidance experiment

We carried out the obstacle avoidance experiment on a flat underwater surface. Fig. 29 shows the walking, detecting, and rotating motions of the microrobot. First, the microrobot walked toward the obstacle using legs A, B, C, and D with a frequency of 1 Hz, and an input voltage of 6 V. When the distance between the microrobot and the obstacle decreased to about 20 mm, three proximity sensors detected the obstacle, as shown in Fig. 29(c). Then the microrobot stopped and rotated clockwise with a frequency of 0.5 Hz, as shown in Fig. 29(d). When the microrobot was rotating clockwise, the right sensor could not detect the obstacle first, then the middle sensor could not detect it, and the last one was the left sensor, as shown in Fig. 29(e) and (f). At this time the microrobot stopped rotating and walked forward, as shown in Fig. 29(g) and (h). Some air bubbles were generated while rotating and walking with a frequency of 0.5 Hz.

6. Conclusions

A new underwater microrobot was introduced with a compact, multi-functional, and flexible structure obtained using ten IPMC actuators as biomimetic legs or fingers. Four actuators were used as legs to implement walking, rotating, and floating motions. The other six actuators were used as fingers to grasp small objects. We analysed the walking mechanism of the robot and modelled the IPMC actuator as a supported cantilever beam. We also analysed the forces applied to one leg and calculated the theoretical walking speed. We then developed a prototype of the microrobot, carried out experiments, and measured the walking speed on a flat underwater surface. The experimental results fit the theoretical results very well. Diving/surfacing experiments were also conducted by electrolysing the water around the actuator surfaces. The microrobot was able to grasp small objects while walking or floating, its most important function. Finally, the microrobot used three proximity sensors to detect the direction and distance of an obstacle, and avoided the obstacle to realise closed-loop control.

Acknowledgement

This research is supported by the Kagawa University Characteristic Prior Research Fund 2011.

References

[1] B. Behkam, M. Sitti, Design methodology for biomimetic propulsion of miniature swimming robots, Journal of Dynamic Systems, Measurement, and Control 128 (1) (2006) 36–43.
[2] W. Zhang, S. Guo, K. Asaka, Development of an underwater biomimetic microrobot with both compact structure and flexible locomotion, Journal of Microsystem Technologies (2006). http://dx.doi.org/10.1007/s00542-006-0294-9.
[3] L. Shi, S. Guo, K. Asaka, A bio-inspired underwater microrobot with compact structure and multifunctional locomotion, in: Proceedings of 2011 IEEE/ASME International Conference on Advanced Intelligent Mechatronics, AIM 2011, Budapest, Hungary, 2011, pp. 203–208.
[4] S. Heo, T. Wiguna, H. Park, N. Goo, Effect of an artificial caudal fin on the performance of a biomimetic fish robot propelled by piezoelectric actuators, Journal of Bionic Engineering 4 (3) (2007) 151–158.
[5] Z. Wang, G. Hang, J. Li, Y. Wang, K. Xiao, A micro-robot fish with embedded SMA wire actuated flexible biomimetic fin, Sensors and Actuators A: Physical 144 (2) (2008) 354–360.
[6] B. Kim, M.G. Lee, Y.P. Lee, Y. Kim, G. Lee, An earthworm-like micro robot using shape memory alloy actuator, Sensors and Actuators A: Physical 125 (2) (2006) 429–437.
[7] S. Liu, T. Huang, J. Yen, Comparison of sensor fusion methods for an SMA-based hexapod biomimetic robot, Robotics and Autonomous Systems 58 (5) (2010) 737–744.
[8] A. Hadi, A. Yousefi-Koma, M.M. Moghaddam, M. Elahinia, A. Ghazavi, Developing a novel SMA-actuated robotic module, Sensors and Actuators A: Physical 162 (1) (2010) 72–81.
[9] M. Shahinpoor, K.J. Kim, Ionic polymer-metal composites: IV. Industrial and medical applications, Journal of Smart Materials and Structures 14 (2005) 197–214.
[10] S. Yeom, I. Oh, A biomimetic jellyfish robot based on ionic polymer metal composite actuators, Journal of Smart Materials and Structures 18 (2009) 1–16.
[11] W. Zhang, S. Guo, K. Asaka, A new type of hybrid fish-like microrobot, International Journal of Automation and Computing 3 (4) (2006) 358–365.
[12] L.N. Hao, S. Xu, B. Liu, A miniature fish-like robot with infrared remote receiver and IPMC actuator, Journal of Northeastern University (Natural Science Edition) 30 (2009) 773–776 (in Chinese).
[13] Q. He, M. Yu, L. Song, H. Ding, X. Zhang, Z. Dai, Experimental study and model analysis of the performance of IPMC membranes with various thickness, Journal of Bionic Engineering 8 (1) (2011) 77–85.
[14] S. Lee, K. Kim, I. Park, Modeling and experiment of a muscle-like linear actuator using an ionic polymer–metal composite and its actuation characteristics, Journal of Smart Materials and Structures 16 (3) (2007) 583–588.
[15] S. Liu, M. Lin, Q. Zhang, Extensional ionomeric polymer conductor composite actuators with ionic liquids, Electroactive Polymer Actuators and Devices (EAPAD), Proceedings of SPIE 6927 (2008) 69270H.
[16] H. Nakadoi, A. Sera, M. Yamakita, K. Asaka, Z. Luo, K. Ito, Integrated actuator-sensor system on patterned IPMC film: consideration of electric interference, in: Proceedings of the 2007 4th IEEE International Conference on Mechatronics, Kumamoto, Japan, 2006, p. 4280007.
[17] N. Kamamichi, M. Yamakita, K. Asaka, Z. Luo, A snake-like swimming robot using IPMC actuator/sensor, in: Proceedings of the 2006 IEEE International Conference on Robotics and Automation, Orlando, United States, 2006, pp. 1812–1817.
[18] B. Kim, D. Kim, J. Jung, J. Park, A biomimetic undulatory tadpole robot using ionic polymer–metal composite actuators, Journal of Smart Materials and Structures 14 (2005) 1579–1585.
[19] B. Gao, S. Guo, X. Ye, Motion-control analysis of ICPF—actuated underwater biomimetic microrobots, International Journal of Mechatronics and Automation 1 (2) (2011) 79–89.
[20] S.T. McGovern, G.M. Spinks, B. Xi, G. Alici, V. Truong, G.G. Wallace, Fast bender actuators for fish-like aquatic robots, Proceedings of SPIE 6927 (2008) 69271L.
[21] W. Yim, J. Lee, K.J. Kim, An artificial muscle actuator for biomimetic underwater propulsors, Journal of Bioinspiration and Biomimetics 2 (2) (2007) S31–S41.
[22] J. Liu, H. Hu, Biological inspiration: from carangiform fish to multi-joint robotic fish, Journal of Bionic Engineering 7 (1) (2010) 35–48.
[23] S. Guo, L. Shi, K. Asaka, L. Li, Experiments and characteristics analysis of a bio-inspired underwater microrobot, in: Proceedings of the 2009 IEEE International Conference on Mechatronics and Automation, Changchun, China, 2009, pp. 3330–3335.
[24] L. Shi, S. Guo, K. Asaka, Development of a new jellyfish-type underwater microrobot, International Journal of Robotics and Automation 26 (2) (2011) 229–241.
[25] L. Shi, S. Guo, K. Asaka, A novel jellyfish- and butterfly-inspired underwater microrobot with pectoral fins, International Journal of Robotics and Automation 27 (3) (2012) 276–286.
[26] http://www.infoplease.com/ce6/sci/A0825073.html.
[27] http://jaredtendlerpoker.com/wp-content/uploads/Inchworm.jpg.
[28] I. Park, S. Kim, D. Kim, K. Kin, The mechanical properties of ionic polymer-metal pomposites, Electroactive Polymer Actuators and Devices (EAPAD), Proceedings of SPIE 6524 (2007) 65241R.
[29] P. Brunetto, L. Fortuna, S. Graziani, S. Strazzeri, A model of ionic polymer–metal composite actuators in underwater operations, Journal of Smart Materials and Structures 17 (2) (2008) 025–029.

[30] W. Liu, X. Jia, F. Wang, Z. Jia, An in-pipe wireless swimming microrobot driven by giant magnetostrictive thin, Sensors and Actuators A: Physical 160 (1) (2010) 101–108.
[31] B. Gao, S. Guo, Development of an infrared ray controlled fish-like underwater microrobot, in: Proceedings of the 2010 IEEE International Conference on Automation and Logistics, Hong Kong & Macau, China, 2010, pp. 150–155.
[32] N.S. Ha, N.S. Goo, Propulsion modeling and analysis of a biomimetic swimmer, Journal of Bionic Engineering 7 (2010) 259–266.
[33] L. Shi, S. Guo, K. Asaka, A novel multifunctional underwater microrobot, in: Proceedings of the 2010 IEEE International Conference on Robotics and Biomimetics, Tianjin, China, 2010, pp. 873–878.
[34] Z. Wang, J. Li, G. Hang, Y. Wang, A flexible hingeless control surface inspired by aquatic animals, Journal of Bionic Engineering 7 (2010) 364–374.
[35] Q. Pan, S. Guo, T. Okada, A novel hybrid wireless microrobot, International Journal of Mechatronics and Automation 1 (1) (2011) 60–69.

Shuxiang Guo (S'93-M'95-SM'03) received the B.S. and the M.S. degrees in mechanical engineering from the Changchun Institute of Optics and Fine Mechanics, Changchun, China, in 1983 and in 1986, respectively, and the Ph.D. degree in mechano-informatics and systems from Nagoya University, Nagoya, Japan, in 1995. In 1995, he was a Faculty Member at Mie University, Mie, Japan and in 1998 at Kagawa University, Kagawa, Japan. Currently, he is a Professor with the Department of Intelligent Mechanical System Engineering at Kagawa University. He has published about 270 refereed journal and conference papers. His current research interests include microrobotics and mechatronics, microrobotics system for minimal invasive surgery, micro catheter system, micro pump, and smart material (SMA, ICPF) based on actuators.

Dr. Guo received research awards from the Tokai Section of the Japan Society of Mechanical Engineers (JSME), the Tokai Science and Technology Foundation, and the Best Paper Award of the IS International Conference, Best Paper Award of the 2003 International Conference on Control Science and Technology and Best Conference Paper Award of IEEE ROBIO 2004, IEEE ICAL 2008 and IEEE ICIA 2011, in 1997, in 1998, in 2000, in 2003, in 2004, in 2008 and in 2011, respectively. He also received the Chang Jiang Professorship Award from Ministry of Education of China, in 2005, and was offered Thousand-Elite-Project in China. He is the founding chair for IEEE International Conference on Mechatronics and Automation. And he is the editor in chief for International Journal of Mechatronics and Automation.

Liwei Shi received the B.S. degree in mechanical engineering from Harbin Engineering University, China, in 2006, the M.S. and the Ph.D. degrees in intelligent machine system from Kagawa University, Japan, in 2009 and in 2012, respectively. Currently, he is a postdoctoral researcher in Kagawa University, Japan. He researches on underwater microrobot utilizing artificial muscles, such as IPMC (ionic polymer metal composite) actuators for industry and biomedical applications. His current research interests include legged bio-inspired microrobots, jellyfish-type underwater microrobots, and spherical underwater robots. He has published about 22 refereed journal and conference papers in the recent three years.

Nan Xiao received his B.Sc. degree from Harbin Engineering University, Heilongjiang, Harbin, China, in 2004, and his M.Sc. degree from Harbin Engineering University, Heilongjiang, Harbin, China, in 2007. Currently, he is a Ph.D. candidate in Kagawa University, Japan. He researches on micro-operating system for biomedical applications, and robotic catheter systems.

Kinji Asaka received the Ph.D. degree in science from Kyoto University in 1991. He is currently a Group Leader of the Artificial Cell Research Group, Research Institute for Cell Engineering of National Institute of Advanced Industrial Science and Technology (AIST). His current research interests include interfacial electrochemistry and polymer actuators. He is a member of the Society of Polymer Science, Japan and The Society of Instrument and Control and Engineers.